

Analysis of martensite–austenite constituent and its effect on toughness in submerged arc welded joint of low carbon bainitic steel

Liangyun Lan · Chunlin Qiu · Dewen Zhao ·
Xiuhua Gao · Linxiu Du

Received: 2 October 2011 / Accepted: 13 February 2012 / Published online: 29 February 2012
© Springer Science+Business Media, LLC 2012

Abstract Martensite–austenite (M–A) constituent formed during welding is generally recognized as an important factor to decrease the toughness of welded joint. In this article, the morphology and chemical composition of M–A constituent in the low carbon bainitic steel welded joint was analysed in detail by means of optical microscope, transmission electron microscope and scanning electron microscope with electron probe microanalysis. The experimental results show that the M–A constituent formed in the different sub-zones presents different morphologies and different amounts. The maximum amount of M–A constituent occurs in the coarse grained heat affected zone (HAZ). It is evident that the carbon atoms segregate on the M–A constituent and carbon concentration on the slender M–A constituent is higher than that on the massive M–A constituent. Meanwhile, the distribution profile of silicon on the M–A constituent shows an obvious inhomogeneity. Most of M–A constituents have a twinned structure and/or a high dislocation density. According to impact testing results, the crack initiation energy in the HAZ specimens deteriorates significantly because the large M–A constituent can assist the formation of cleavage crack. On the other hand, the coarse prior austenite grain in the HAZ lowers the crack propagation energy.

Introduction

In recent decades, the submerged arc welding technique has been widely applied in the welding field of high strength

structural steel, e.g., pipeline, pressure vessels, box columns, offshore structure [1, 2]. However, although the base metal (BM) has an excellent combination of high strength and toughness, the deterioration phenomenon of toughness of welded joint always occurs after welding, especially for large heat input processing. It is generally accepted that the deterioration in toughness of welded joint has a close relationship with microstructural characteristics, such as martensite–austenite (M–A) constituents, non-metallic inclusions, prior austenite grain size as well as the fraction of acicular ferrite in the matrix microstructure [1–8].

Considerable research has focused on the deleterious effect of M–A constituent on simulated heat affected zone (HAZ) toughness. For example, Davis and King [5] have shown that cleavage crack initiation mainly depends on the distribution and morphology of M–A constituent in the simulated intercritically reheated HAZ (ICHAZ) and concluded several possible micromechanisms of M–A constituent causing a reduction in HAZ toughness. Li et al. [6] have shown that the ICHAZ toughness does not deteriorate drastically for the API X70 pipeline steels because the size of M–A constituent is small and the content of M–A constituent is relatively little for the effect of accelerating cooling. The alloying addition (e.g., Nb) had a significant effect on the amount and size of the M–A constituent and those constituents further deteriorated the toughness of simulated ICHAZ [7]. In addition, Moeinifar et al. [8] have studied the variation of M–A particles in the ICHAZ by means of Gleeble simulation technique and real tandem submerged arc welding and concluded that the fraction and morphology of M–A constituent as well as the prior austenite grain size are important factors on the Charpy impact energy in the ICHAZ.

As stated above, it is evident that the M–A constituents in the welded joint play an important role in decreasing the toughness, especially for crack initiation energy. Most of these

L. Lan (✉) · C. Qiu · D. Zhao · X. Gao · L. Du
State Key Laboratory of Rolling and Automation, Northeastern University, P.O. Box 105, No.11, Lane 3, Wenhua Road, HePing District, Shenyang 110819, People's Republic of China
e-mail: lly.liangyun@gmail.com

Table 1 Chemical compositions and as-rolled mechanical properties of the low carbon bainitic steel

Chemical compositions (wt%)						Mechanical properties				
C	Si	Mn	Nb + V + Ti	B (ppm)	Others	P_{cm}	$R_{10.5}$ (Mpa)	R_m (Mpa)	A (%)	Toughness (−20 °C)
0.053	0.27	1.35	0.082	12	Cr, Mo, Ni	0.185	640	760	18	161 J

studies were carried out by the welding thermal cycle simulation technique because it can be used to generate a relatively large region for special sub-zone [7]. However, this technique also has its own limitations, such as single simulation microstructure cannot reflect completely the continuous variation of real HAZ microstructure and the weld metal (WM) columnar microstructure is hard to be simulated because it cools directly from the liquid [9]. The characters of M–A constituent in different sub-zones of the real welded joint must be different because the welded joint is subjected to uneven welding thermal cycle. Therefore, the M–A constituent should be studied in detail to further understand its effect on the cleavage fracture micromechanism. Meanwhile, the formation of M–A constituent is associated with the segregation of many elements, such as carbon and silicon [10]. These segregated elements may have different distribution profiles on the M–A constituents formed in different sub-zones, which, in turn, may influence the amounts and morphologies of M–A constituents. However, very few studies have focused on the microsegregation of composition on the M–A constituent. Therefore, in this study, more attention has been paid to the morphology and chemical composition segregation of M–A constituent in different sub-zones of real welded joint. In addition, the effect of M–A constituent on the impact toughness has been also discussed to further understand the cleavage fracture micromechanism in the welded joint.

Experimental procedure

The low carbon microalloyed steel with the thickness of 20 mm was produced in the as-rolled condition by

thermo-mechanical control process (TMCP). The chemical compositions and mechanical properties of this steel are shown in Table 1. To protect the welded joint from welding cold crack, the carbon content and welding crack susceptibility index P_{cm} designed are 0.053 and 0.183%, respectively, and P_{cm} was given by Eq. 1 [11].

$$P_{cm} = C + \frac{Si}{30} + \frac{Mn + Cu + Cr}{20} + \frac{Ni}{60} + \frac{Mo}{15} + \frac{V}{10} + 5B \tag{1}$$

According to the standard of EN ISO 9692 [12], a single V-type butt weld groove was designed for the experimental steel plate with size of 20 (thickness) × 100 (width) × 400 (length) mm which was cut along the longitudinal direction of hot rolled steel. Four-pass welding procedure was conducted to generate a relatively wide HAZ region. The main welding parameters were: current 600 A, voltage 30 V, welding speed 40 cm/min, inter-pass temperature range 180–200 °C and the corresponding heat input was about 27 kJ/cm. Low alloy steel electrodes (H08MnMoNiA) with 4.0 mm in diameter were used for submerged arc welding according to Chinese welding standard of GB/T 12470 [13]. An agglomerated commercial flux was selected which contained Al₂O₃, SiO₂, MnO, CaO, CaF₂, TiO₂.

After welding, impact specimens with standard size were prepared along the transversal direction of welding passes. In order to fix the right position of Charpy V notch, the impact specimens were macro-etched with 3% nital first to exhibit the outline of HAZ. According to ISO 9016 standard [14], the Charpy V notch position was fixed at different regions of welded joint to examine the toughness of these regions as shown in Fig. 1. Because of the narrow

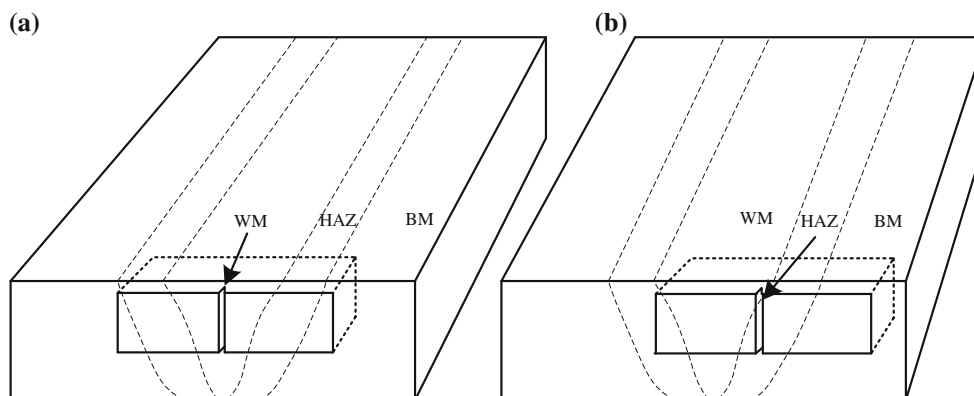


Fig. 1 Schematic diagram of Charpy V notch positions at the WM (a) and HAZ (b)

width of sub-zones in HAZ, the Charpy V notch in the HAZ was across the whole of coarse grained HAZ (CGHAZ) and a part of fine grained HAZ (FGHAZ). The impact testing was carried out at $-20\text{ }^{\circ}\text{C}$ and each region was tested at least five times. An instrumented drop-weight impact tester was employed to record the impact load–deflection curves. The impact absorbed energy can be divided into crack initiation energy and crack propagation energy based on these impact curves [15, 16].

The metallographic specimen was cut from the welded plate on transverse section with respect to the welding direction, which was parallel to the rolling direction. The polished specimen was etched with 3% nital for optical microscope and scanning electron microscope (SEM) observation. To identify the morphology and amount of M–A constituent in different sub-zones of HAZ, the specimen was repolished and etched with LePera reagent. The segregation of composition on the M–A constituent was examined using electron probe micro-analysis (EPMA) attached to a field-emission SEM. Thin-foil specimens for transmission electron microscope (TEM) were prepared to observe the refinement microstructure at different regions in welded joint. Fracture surface morphology of impact specimens were also examined with the SEM. The statistical analysis on the amount and size of M–A constituents was conducted using an image analyzer based on optical and SEM micrographs.

Results and discussion

Microstructural characteristics in different sub-zones

Figure 2 shows the microstructural characteristics at different regions in the welded joint after subjected to multi-pass welding process. The overall microstructure at the low magnification condition is shown in Fig. 2a, which contains five different sub-regions: BM, ICHAZ, FGHAZ, CGHAZ, and WM designated with number square grids. The corresponding higher magnification microstructures are showed in the following figures from Fig. 2b–f. The BM microstructure consists mainly of granular bainite and a small amount of quasi-polygonal ferrite with the dispersive distribution of second phase (Fig. 2b) due to subjected to low welding temperature (peak temperature below A_{c1}). The ICHAZ has a mixture of untransformed granular bainite and quasi-polygonal ferrite as well as retransformed martensite islands or M–A constituents which form at the grain boundaries (Fig. 2c). The microstructure of FGHAZ is predominantly quasi-polygonal ferrite with very small grain size (Fig. 2d), mainly due to complete re-austenitisation at relatively low peak temperatures and for short periods of time. The mean grain size in FGHAZ is about $5.4\text{ }\mu\text{m}$ roughly measured by the line intercept method. The

CGHAZ has lath or granular bainite with large prior austenite grain size (Fig. 2e). The maximum size of prior austenite grain measured can reach about $300\text{ }\mu\text{m}$. Acicular ferrite and proeutectoid grain boundary ferrite are present at regular intervals in the WM region and some of inclusions are signified by arrows (Fig. 2f). The WM microstructure begins to solidify by epitaxial growth of columnar delta-ferrite from the parent plate at the fusion line, and then the austenite grains form during further cooling. The grain boundary ferrite forms at the columnar austenite grain boundaries by a carbon diffusion mechanism and subsequently, acicular ferrite nucleates and grows with a displacement mechanism attached to granular inclusions inside the columnar austenite grain [17].

TEM study of detailed microstructures in different sub-zones

The detailed morphology of microstructures in welded joint studied by TEM is presented in Fig. 3. Figure 3a shows that acicular ferrite plates in the WM are arranged in an interlocking pattern due to hard impingement and some acicular ferrite plates seem to nucleate on the granular inclusions arrowed in Fig. 3a. These granular inclusions have the characteristics of complex oxides as they are composed of many elements including Ti, Al, Mn, Si, O, and S shown by the EDS in Fig. 3b. As these inclusions can greatly influence the formation of acicular ferrite which contributes to enhancing toughness due to its high angle boundaries, many researchers have concentrated on the role of inclusions in stimulating the nucleation of acicular ferrite [3, 4, 18]. Thewlis et al. [18] proposed that the amount of acicular ferrite transformed mainly depends on the inclusion type in WM because an absence of inclusions TiN or MnS can lead to reduce acicular ferrite. Fig. 3c reveals the coarse parallel laths of bainite structure in the CGHAZ, accompanied with many small M–A constituents distributing among the bainite lath boundaries. These M–A constituents are further discussed later. The bainite laths contain a high dislocation density mainly resulting from uneven phase transformation by a shear mechanism [19]. The TEM micrographs in FGHAZ consisting of polygonal ferrite (or massive ferrite) with small grain size are presented in Fig. 3d. The polygonal ferrite has curved irregular grain boundaries and relatively lower dislocation density because of microstructure occurring completely recrystallization in the FGHAZ.

Morphology, micro-composition, and structure of M–A constituents in different sub-zones

After the metallurgical specimen was etched with the LePera reagent for about 20 s, the M–A constituents appear

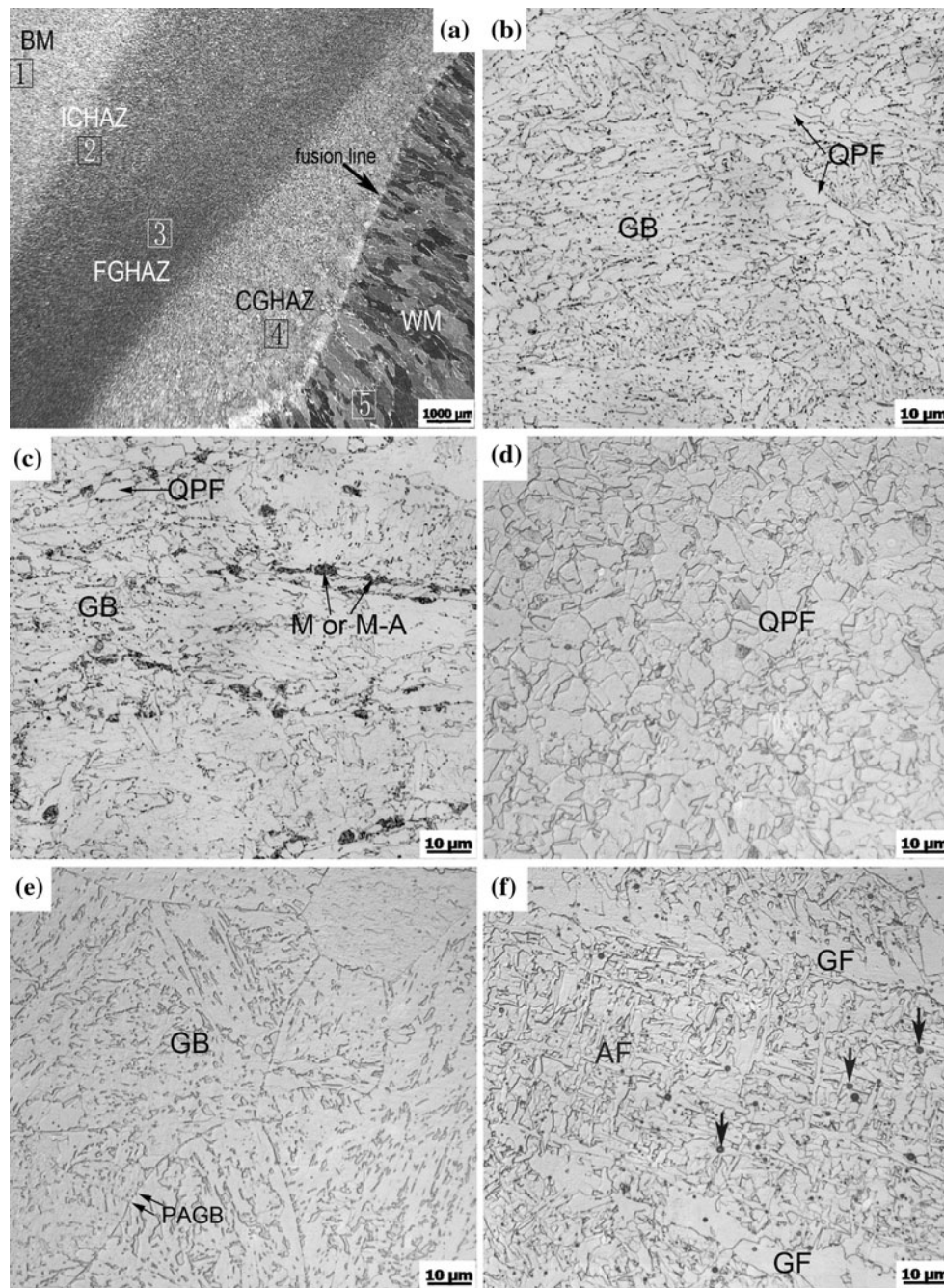


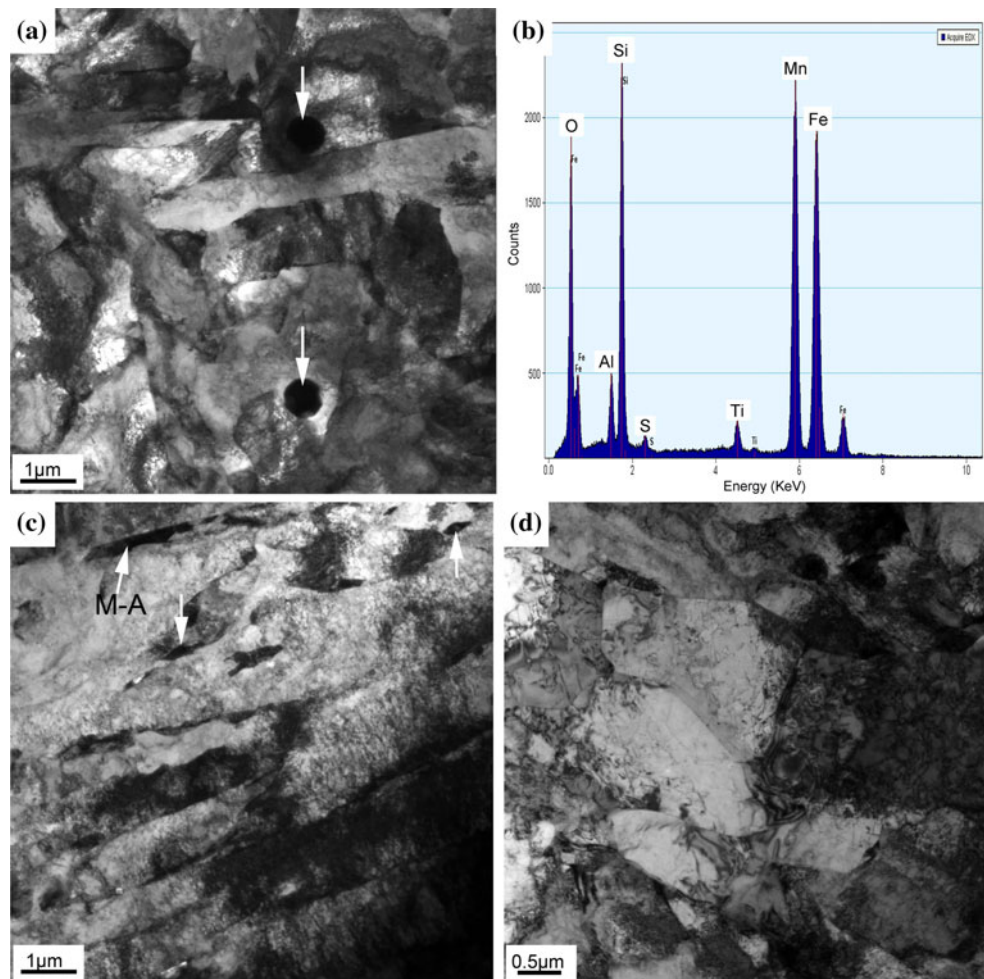
Fig. 2 Optical micrographs showing the microstructures in different regions of the welded joint **a** low magnification overall microstructure, **b** BM (or tempered zone), **c** ICHAZ, **d** FGHAZ, **e** CGHAZ,

f WM (*GB* granular bainite, *QPF* quasi-polygonal ferrite, *M* martensite, *M–A* martensite–austenite constituent, *PAGB* prior austenite grain boundary, *AF* acicular ferrite, *GF* grain boundary ferrite)

white, while inclusions and carbides are black, as shown in Fig. 4. In the WM (Fig. 4a), only a few M–A constituents have a relatively large size (maximum length more than 2 μm) and most M–A constituents have a very small size with dot shape (less than 1 μm). Because of the formation of acicular ferrite by a shear mechanism, carbon enrichment always occurs at the boundaries of acicular ferrite. Therefore, most of the M–A constituents are distributed

along the acicular ferrite boundaries. As shown in Fig. 4b, many M–A constituents in the CGHAZ have a conspicuous character of slender shape with the high aspect ratio (the ratio of maximum length to width). The maximum length of M–A constituent measured can reach about 25 μm. Those slender M–A constituents delineate the bainite lath boundaries inside the large prior austenite grain. Several large massive M–A constituents as well as many relatively

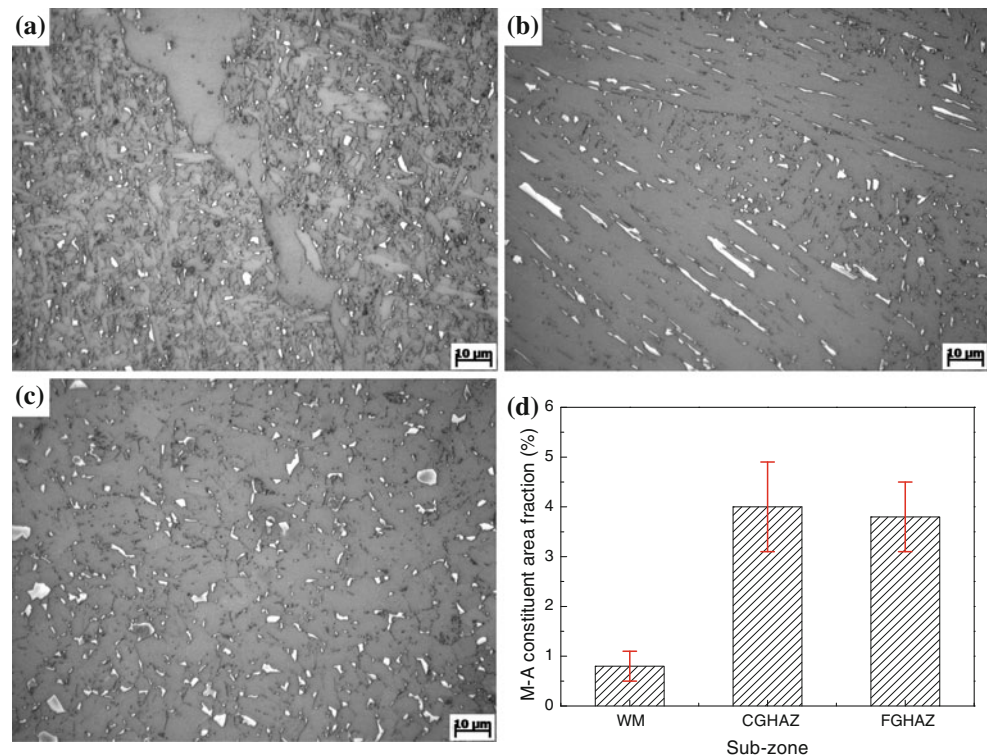
Fig. 3 TEM micrographs showing refinement microstructures at different regions in the welded joint **a** WM, **b** chemical composition of inclusions in the WM, **c** CGHAZ, **d** FGHAZ



small irregular M–A constituents are represented in the FGHAZ, as shown in Fig. 4c. It can be found that the irregular M–A constituents are also prone to form along the boundaries of massive ferrite because the formation of massive ferrite is controlled by carbon diffusion. Optical micrographs were processed with an image analyzer as per the method proposed by Bonnevie et al. [20]. All the micrographs were transformed into binary images to calculate the area fraction of M–A constituent easily. As shown in Fig. 4d, the average area fraction of M–A constituent in the WM, CGHAZ and FGHAZ is about 0.8 ± 0.3 , 4.0 ± 0.9 , and $3.8 \pm 0.7\%$, respectively. It is evident that the amount and morphology of the M–A constituent formed in different sub-zones is directly determined by welding thermal cycle experienced. Moreover, the formation of M–A constituent is also inseparable from segregation of chemical composition in these micro-zones. Some researches have shown that some micro-elements added in steel can obviously enhance the amount of M–A formation [7, 10, 20]. Therefore, micro-elements segregated on the M–A constituent were analyzed with EMPA and discussed in the following paragraph.

The EPMA line scanning method can be used for qualitative and semi-quantitative analysis of chemical composition segregated on the M–A constituent as shown in Fig. 5. Figure 5a shows the SEM microstructure in the WM at high magnification. The scanning line signified with a black arrow line in Fig. 5a is across three acicular ferrite grains and two small M–A constituents and the corresponding elemental distribution profiles are shown in Fig. 5b, in which the relative counts of the element represent qualitatively the concentration distribution of element along the scanning line. It can be seen that the carbon concentration in the M–A constituent is at least twice that in the acicular ferrite matrix. On the contrary, the segregation of silicon in the M–A constituents seems to be controlled by a short range diffusion mechanism, which shows that the peak concentration of silicon occurs in the M–A constituent near the one side of constituent boundary and the lowest concentration appears at the other side of the M–A constituent/matrix interface, as shown in Fig. 5b. Meanwhile, the concentration of substitutional elements, such as Mn, Ni, does not exhibit any obvious change on the M–A constituents and their distribution profiles are not

Fig. 4 Morphology and area fraction of M–A constituent in different sub-zones **a** WM, **b** CGHAZ, **c** FGHAZ, **d** area fraction of M–A constituent



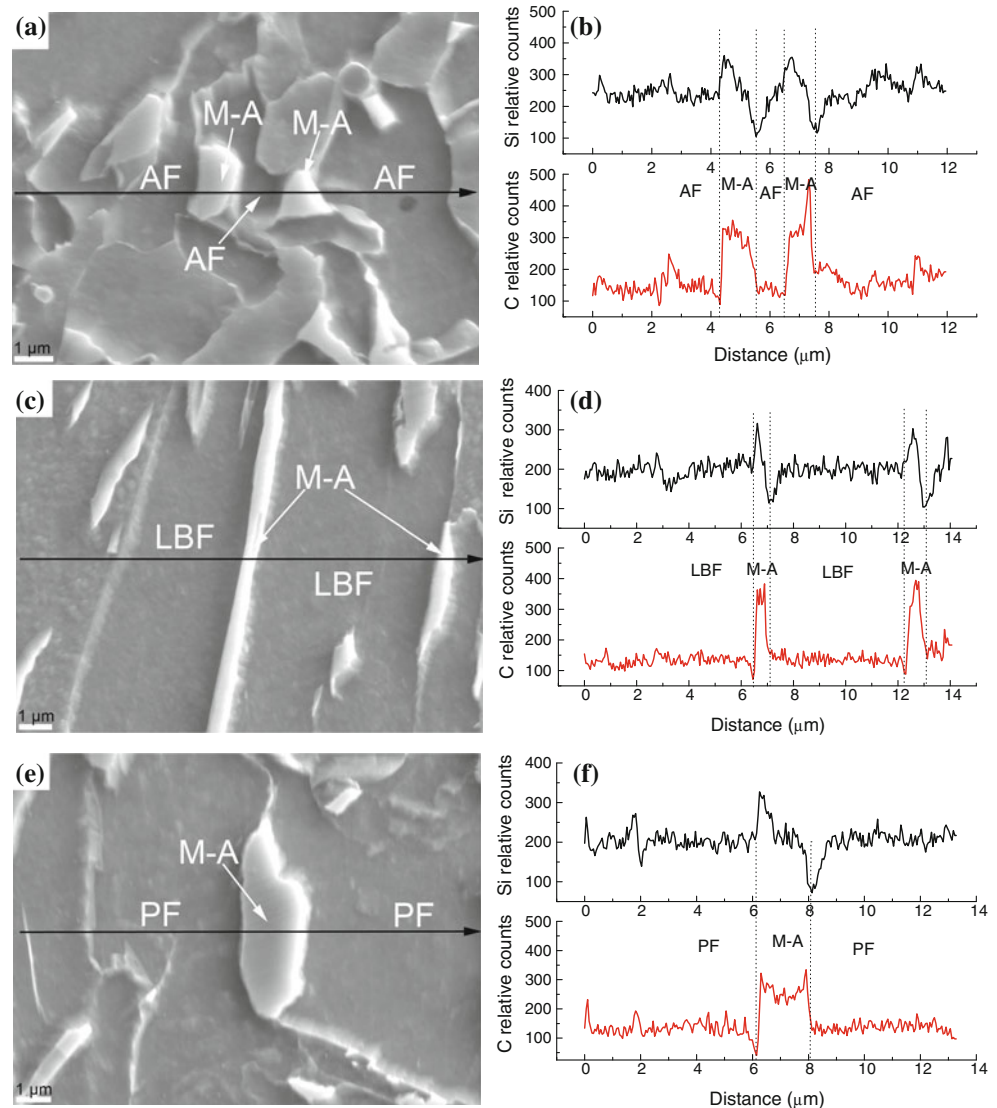
given. Figure 5c shows the slender M–A constituents in the lath bainite matrix of the CGHAZ and corresponding carbon and silicon concentration distributions along the scanning line are shown in the Fig. 5d. It can be found that the carbon concentration is higher and the larger concentration gradient of silicon is still presented on the slender M–A constituents compared with the massive M–A constituent. The SEM micrograph and corresponding carbon and silicon distribution profiles from the massive M–A constituents in the polygonal ferrite matrix of the FGHAZ are shown in Fig. 5e and f, respectively. A similar concentration distribution trend of carbon and silicon can be obtained from the FGHAZ massive M–A constituent, the carbon concentration at the periphery of the massive M–A constituent seems to be higher than that in its middle region and the silicon concentration in the center of the massive M–A constituent equals the matrix silicon concentration.

The occurrence of carbon segregation is a necessity to the formation of M–A constituent because carbon enrichment in the residual austenite at the last stage of phase transformation can notably enhance the stability of residual austenite and decrease the martensite start temperature (M_s) at these local zones. Biss and Cryderman [10] have reported that the high carbon peaks on the M–A constituent often exceeded 0.5 wt% and occasionally exceeded 1 wt%. Santofimia et al. [21] have proposed that the carbon concentration ranged from value close to zero in ferrite to up to 1.2 wt% in the M–A constituents after the low carbon steel was subjected to intercritical annealing treatment.

According to the EMPA line scan analysis, after welding, carbon is clearly concentrated on the M–A constituent compared with the matrix. The concentration of carbon in the slender M–A constituent seems to be higher than that in the massive M–A constituent. Meanwhile, the carbon distribution profile at the massive M–A constituents in the FGHAZ shows that the carbon concentration at the periphery is usually higher than that in the center.

As regards the silicon distribution of the M–A constituent, because of the lower diffusion coefficient of silicon compared to carbon atoms, the segregation of silicon on the M–A constituent is not as obvious as the carbon segregation. However, there is a repulsive force between silicon and carbon atoms. High silicon content in ferrite can promote the carbon enrichment of the M–A constituent. On the other hand, silicon segregated at the interface of untransformed austenite can greatly retard the formation of carbides in austenite as well as in ferrite [22]. Therefore, the increase of silicon content in steel can slow down the decomposition of retained austenite and increase the amount of M–A constituent [20, 22]. According to the EPMA line scan results, it can be found that the carbon and silicon atoms are concentrated in the M–A constituent in the welded joint. This is consistent with the results of Pereloma et al. [23]. They have studied the distributions of carbon and silicon in the various matrix phases of TRIP steels by using three dimensional atom probe analysis and concluded that the highest concentrations of carbon and silicon occur on the residual austenite phase.

Fig. 5 SEM micrographs showing morphology of M–A constituent and corresponding EMPA analysis of element segregated on the M–A constituent in different sub-zones **a** WM microstructure, **b** corresponding carbon and silicon distribution profiles in the WM, **c** CGHAZ microstructure, **d** corresponding carbon and silicon distribution profiles in the CGHAZ, **e** FGHAZ microstructure, **f** corresponding carbon and silicon distribution profiles in the FGHAZ



As stated above, the M–A constituents formed at different sub-zones have some differences in the distribution of segregated elements and morphology, which may reflect the wide variety of M–A constituents in nature. Some researchers have classified the M–A constituent in low carbon steels into three groups [20, 24]: one group is fully martensite constituents with microtwins and/or high dislocation density, the second group is fully retained austenite with pile-up defects, and the third group is mixed constituents associating with austenite and martensite. In the mixed M–A constituents, austenite is distributed at the periphery, while martensite is located at the center reported by Lambert et al. [24], which seems to correspond to the carbon gradient on the massive M–A constituents in the FGHAZ because carbon content is higher at the periphery of the massive M–A constituents (Fig. 5f).

However, it is generally accepted that fully twin martensite is often obtained in the HAZ not only

because of inhomogeneity of carbon concentration in the austenite grains but also due to the various cooling rates and thermal stresses in the HAZ [25]. According to the selected area diffraction (SAD) analysis as shown in the Fig. 6, the typical fully martensite phase occurred in the CGHAZ and the cycled area showed the micro-zone of SAD analysis (Fig. 6a). The corresponding SAD pattern, with a [113] zone axis, showed the twinning relationship between the parallel martensite laths and the matrix (Fig. 6b). These transformation twin martensites can relieve high thermal, solidification induced and transformation induced stresses [25]. Meanwhile, the amount of M–A constituent existing in the form of fully retained austenite should be very little mainly because of low carbon content in this steel. Thus, most M–A constituents in the welded joint have a character of twinning structure and/or high dislocation density [8, 25].

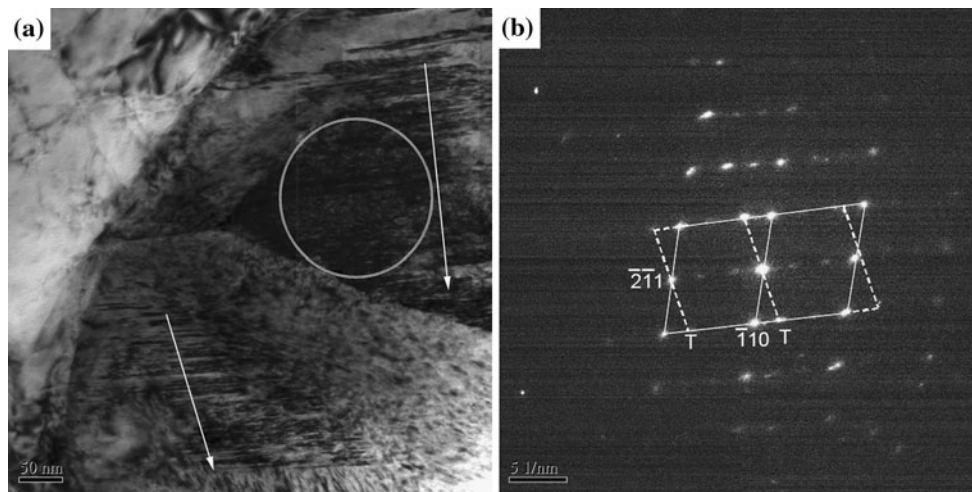


Fig. 6 TEM micrograph showing a twinning structure of M–A constituent in the CGHAZ **a** the morphology of M–A constituent with typical micro-twins signified by *arrows* and a twin region cycled for SAD analysis, **b** corresponding SAD pattern of twinned martensite from (a)

Toughness and fracture morphologies in different sub-zones of welded joint

Impact load–deflection curves as well as impact absorbed energy–deflection curves can be recorded by means of the instrumented Charpy impact tester [15, 16, 26]. Figure 7 shows the typical instance of impact curves of the HAZ impact specimen. It can be seen that the impact load decreases sharply after it reach the peak value and the total impact absorbed energy is about 58 J. Fig. 8 shows that the toughness of the welded joint deteriorated significantly compared with the toughness of the BM specimens. Both the crack initiation energy and the crack propagation energy in the welded joint decrease simultaneously. The lowest values of crack initiation and propagation energies are obtained for the HAZ specimens.

In general, the amount of acicular ferrite and inclusions in the WM are mainly responsible for the WM toughness.

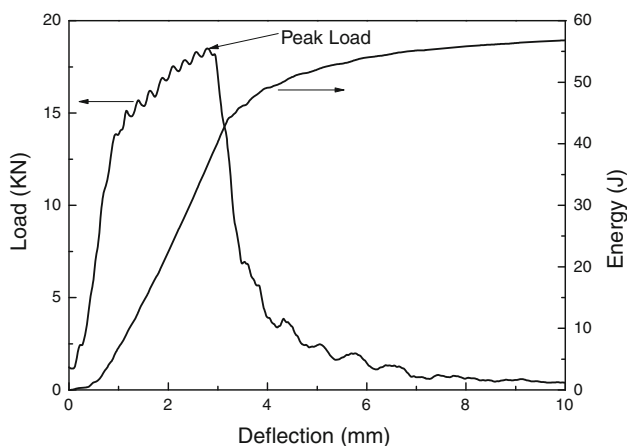


Fig. 7 Typical curves of impact load–deflection and impact absorbed energy–deflection of the HAZ specimen

High volume fraction of acicular ferrite in the WM matrix can obviously enhance the impact toughness because of its high angle grain boundaries and interlocked arrangement in nature as shown in Fig. 3a. However, the amount of acicular ferrite formed in the WM can be influenced by various factors, e.g., welding parameters, alloying elements, and inclusions [1, 3, 17, 18, 27]. Viano et al. [1] concluded that the volume fraction of acicular ferrite decreased as the heat input increased and heat input also had a significant effect of the acicular ferrite lath width. Thus, high heat input adversely affected the impact toughness. Under the present welding parameters, the acicular ferrite as well as grain boundary ferrite can be formed simultaneously in the WM. The corresponding fracture surface is shown in Fig. 9a. It can be seen that the WM fracture surface exhibits the typical quasi-cleavage fracture features which contains a mixed morphologies of ductile and brittle fracture. Figure 9b shows magnified ductile fracture morphology

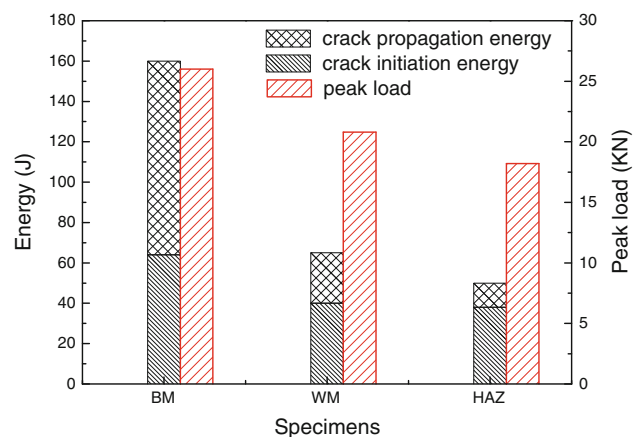


Fig. 8 Average impact absorbed energy and peak load of specimens with different Charpy V notch positions

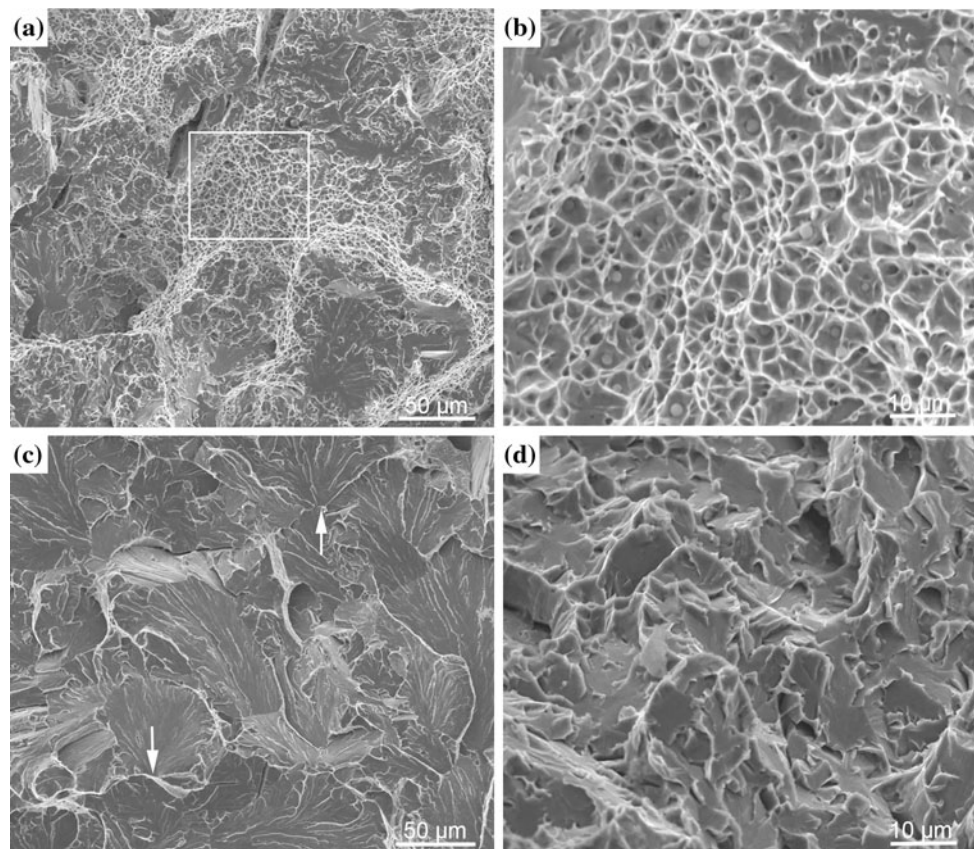


Fig. 9 SEM micrographs showing the fracture surface morphology of specimens with different Charpy V notch positions **a** WM fracture surface morphology, **b** magnified ductile fracture morphology

corresponding to the square grid region in (a). **c** CGHAZ cleavage fracture morphology in the HAZ specimen, and **d** FGHAZ cleavage fracture morphology in the HAZ specimen

corresponding to the square grid region in Fig. 9a. According to fracture surface features, there are many inclusions inside the dimples and on the cleavage facets, which indicate that both microvoid coalescence and cleavage fracture are strongly influenced by the non-metallic inclusions in the WM. Tweed et al. [27] suggested that cracked inclusions above a certain size (about 1 μm) lead to the initiation of ferrite cleavage which propagates preferentially through grain boundary ferrite in the WM. Avazkonandeh-Gharavol et al. [17] proposed similar conclusions, i.e., that if inclusions do not provide efficient sites for nucleation of acicular ferrite, they are detrimental to toughness especially for inclusions greater than 1 μm in diameter. The M–A constituent is also an important factor in influencing the toughness in the WM. However, the small size and low volume fraction of M–A constituents in the WM as shown in Fig. 4 may reduce their deleterious effect.

According to impact results as shown in Fig. 8, the HAZ toughness deteriorated significantly compared to the BM toughness. It is generally recognized that the M–A constituents formed in the HAZ have a significant negative effect on the toughness of the welded joint [5–8, 17, 23,

24]. The fractions of M–A constituent formed in the CGHAZ and FGHAZ are about 4.0 and 3.8%, respectively. Most of these M–A constituents have a twinned martensitic structure with high contents of carbon and silicon, as shown by the EPMA and TEM analyses. Thus, the hardness of M–A constituents is very high compared with the matrix. When an impact load is applied to the welded joint containing M–A constituents having a large size, an excessive internal stress will be generated in the matrix near the M–A constituent because of the concentration of plastic strains resulting from the mismatching of their hardness [28]. The concentration of plastic strains near the M–A constituent plays an important role in the initiation of cleavage crack. The fracture surface morphologies of the CGHAZ and FGHAZ in the HAZ specimen are shown in Fig. 9c and d, respectively. It can be seen that the cleavage crack initiates near the M–A constituents attached to prior austenite boundaries arrowed in the Fig. 9c. Because of the large prior austenite grain size in the CGHAZ, the unit cleavage facet with a large size present on the fracture surface contributes to lowering the crack propagation energy. The cleavage facets in the FGHAZ seem to initiate near the M–A constituent along the grain boundaries,

although the size of unit cleavage facet is rather small (Fig. 9d). However, the lowest crack initiation energy for the HAZ specimens is mainly attributed to large M–A constituents in the CGHAZ, because the cleavage fracture micromechanism of coarse bainite is largely controlled by the crack initiation stage according to previous research [26].

In addition to the high volume fraction of M–A constituent which can significantly lower the toughness, the morphology of M–A constituent is also an important factor influencing the toughness. Davis and King [5] reported the lowest impact toughness of simulated ICHAZ was associated with a particular microstructure containing a near-connected grain boundary network of blocky M–A particles. Due to the M–A particles being significantly harder than the internal grain microstructure, the crack initiates easily between two closely spaced M–A constituents. From a fractographic examination, Li and Baker [29] concluded that the elongated stringer M–A particles were more likely to debond from the matrix while the blocky M–A particles were more likely to crack. Moreover, Moeinifar et al. [30] who studied the microstructure evolution of welding HAZ with different cooling rates by the multiple tandem submerged arc welding process and thermal simulated welding technique, concluded that the size of M–A constituents, such as the mean diameter and length, is an important factor influencing Charpy impact properties of CGHAZ and the microcrack nucleation may occur from M–A particles at the intersection of prior austenite grain boundaries. The large slender shape M–A constituents in the CGHAZ distributing along the prior austenite grain boundaries or lath packet boundaries can notably promote the formation of microcrack (Fig. 9c). The M–A constituents with massive shape in the FGHAZ can also assist the initiation of cleavage crack (Fig. 9d). Therefore, the crack initiation energy of HAZ samples is obviously lower than that of BM. On the other hand, the large prior austenite grain size can greatly decrease the crack propagation energy because of the increasing unit cleavage crack facet size.

Conclusions

(1) After the welded joint was subjected to multi-pass submerged arc welding process, most M–A constituents formed in the WM have a small size and are always distributed along the acicular ferrite boundaries. On the contrary, quite a number of M–A constituents exhibit long slender shape in the CGHAZ, which delineates the bainitic ferrite lath boundaries inside the large prior austenite grains. In the FGHAZ, some M–A constituents with large massive shape are distributed in the polygonal ferrite matrix.

- (2) Carbon concentration on the slender M–A constituent is higher than that on the massive M–A constituent and the carbon content at the periphery of massive M–A constituent is slightly higher than that in the center of massive M–A constituent. Meanwhile, the distribution profile of silicon on the M–A constituent shows an obvious inhomogeneity.
- (3) Most M–A constituents formed in the welded joint are fully martensite constituents with a twinned structure and/or a high dislocation density.
- (4) The M–A constituents with large size can greatly decrease the crack initiation energy in the HAZ because they can stimulate the formation of cleavage crack, while the deterioration effect of M–A constituent on the WM toughness may weaken because of their small size.

Acknowledgements The present study is supported by the National Natural Science Foundation of China (No. 51074052) and the Fundamental Research Funds for the Central Universities (N100607001).

References

1. Viano DM, Ahmed NU, Schumann GO (2000) *Sci Technol Weld Join* 5(1):26
2. Kojima A, Yoshii K, Hada T, Saeki O, Ichikawa K, Yoshida Y, Shimura Y, Azuma K (2004) *Nippon Steel Tech Report* 90:39
3. Koseki T, Thewlis G (2005) *Mater Sci Technol* 21:867
4. Ricks RA, Howell PR, Barritte GS (1982) *J Mater Sci* 17:730. doi:10.1007/BF00540369
5. Davis CL, King JE (1994) *Metall Mater Trans A* 25:563
6. Li C, Wang Y, Chen Y (2011) *J Mater Sci* 46:6424. doi:10.1007/s10853-011-5592-7
7. Li Y, Crowther DN, Green MJW, Mitchell PS, Baker TN (2001) *ISIJ Int* 41:46
8. Moeinifar S, Kokabi AH, Hosseini HRM (2011) *Mater Des* 32:869
9. Harrison PL, Farrar RA (1989) *Int Mater Rev* 34:35
10. Biss V, Cryderman RL (1970) *Metall Trans* 2:2267
11. De Meester B (1997) *ISIJ Int* 37:537
12. EN ISO 9692-2 (1998) *Welding and allied processes-joint preparation: Part 2: submerged arc welding of steels*
13. GB/T 12470 (2003) *Low-alloy steel electrodes and fluxes for submerged arc welding (Chinese Standard)*
14. ISO 9016 (2001) *Destructive tests on welds in metallic materials-impact tests-test specimen location, notch orientation and examination*
15. Wiesner CS (1996) *Int J Pres Ves Pip* 69:185
16. Cvetkovski S, Adziew T, Adziew G, Sedmak A (2002) *Eur Struct Integr Soc* 30:95
17. Avazkonandeh-Gharavol MH, Haddad-Sabzevar M, Haerian A (2009) *J Mater Sci* 44:1902. doi:10.1007/s10853-009-4141-0
18. Thewlis G, Chao WT, Harrison PL, Rose AJ (2008) *Mater Sci Technol* 24:771
19. Bhadeshia HKDH, Christian JW (1990) *Metall Trans A* 21A:767
20. Bonnevie E, Ferriere G, Ikhlef A, Kaplan D, Orain JM (2004) *Mater Sci Eng A* 385:352
21. Santofimia MJ, Kwakernaak C, Sloof WG, Zhao L, Sietsma J (2010) *Mater Charact* 61:937

22. Taillard R, Verrier P, Maurickx T, Foct J (1995) *Metall Mater Trans A* 26A:447
23. Pereloma EV, Timokhina IB, Miller MK, Hodgson PD (2007) *Acta Mater* 55:2587
24. Lambert A, Drillet J, Gourgues AF, Sturel T, Pineau A (2000) *Sci Technol Weld Join* 5:168
25. Poorhaydari K, Patchett BM, Ivey DG (2006) *Mater Sci Eng A* 435–436:371
26. Lan L, Qiu C, Zhao W, Gao X, Du L (2011) *Mater Sci Eng A* 529:192
27. Tweed JH, Knott JF (1987) *Acta Metall* 35:1401
28. Matsuda F, Ikeuchi K, Fukada Y, Horii Y, Okada H, Shiwaku T, Shiga C, Suzuki S (1995) *Trans JWRI* 24:1
29. Li Y, Baker TN (2010) *Mater Sci Technol* 26:1029
30. Moeinifar S, Kokabi AH, Madaah Hosseini HR (2011) *J Mater Process Technol* 211:368